GUST RESPONSE: A VALIDATION EXPERIMENT AND PRELIMINARY NUMERICAL SIMULATIONS

Holger Mai[1], Jens Neumann[2], Holger Hennings[3]

[1] Team Leader
Institute of Aeroelasticity of the German Aerospace Center (DLR)
Bunsenstr. 10, 37073 Goettingen, Germany
holger.mai@dlr.de

[2] Scientist
Institute of Aeroelasticity of the German Aerospace Center (DLR)
Bunsenstr. 10, 37073 Goettingen, Germany
jens.neumann@dlr.de

[3] Head of Department
Institute of Aeroelasticity of the German Aerospace Center (DLR)
Bunsenstr. 10, 37073 Goettingen, Germany
holger.hennings@dlr.de

Keywords: gust simulation, forced response, fluid-structure interaction, wind-tunnel experiment

Abstract: In this paper the experimental setup and first results for a gust generator experiment will be presented. The experiment was carried out in the transonic wind-tunnel facility in Goettingen (DNW-TWG). The first goal of the experiment was to answer the question, whether it is possible to induce an unsteady flow field with a rigid moving profile as a gust generator. Furthermore the main objective of the experiment was the understanding of the physical phenomena of an impacting gust on an elastic structure. For that purpose a new set-up has been constructed and built, which allows the investigation of two subsequent airfoil-models in the flow of the wind tunnel. The first airfoil is active and should produce a generic gust. The second model located downstream is passive and responds to the unsteady load changes induced by the moving active profile. For a first investigation, amplitudes and frequencies were varied as well as the vertical position of both airfoils relative to each other.
The experiment was conducted to deliver a comprehensive data base for validating the DLR in-house fluid-structure-interaction software "PyCSM" which has been developed for aeroelastic simulations in time domain.
In order to support the experiment in the preparation phase, fluid-structure-interaction simulations in time domain have been carried out. These simulations mainly show the response amplitudes expected for the passive wing. For that purpose the DLR TAU Code for the calculation of the steady and unsteady aerodynamic loads and a finite element shell model have been used.

1 INTRODUCTION

The investigation of the general gust problematic for any kind of aircraft has become one of the most important fields in aeroelastic experiments and simulations in the last years. Due to the sudden occurring load changes during a gust encounter, the loads on different structure elements, like wings or horizontal tail planes, can become very high. Therefore an accurate prediction of such time dependent loads is very important for modern aircraft design to

ensure structural integrity and to avoid unstable flight conditions [1]. But not only general gusts can influence the structural behaviour and cause vibrations. Also the wake of the wing can produce an unsteady flow field with frequencies which in turn can excite a downstream lying horizontal tail plane. To handle such strong load changes, experimental and numerical investigation must be accomplished first for a better understanding of the physical phenomena and second to improve our mathematical modelling to increase load prediction. In the following this may lead to the design of better active load control systems and hence an active load reduction to increase passenger comfort and reduce fatigue.
For the validation of high fidelity numerical codes, a reference data set is needed. Unfortunately only few wind-tunnel experiments have been reported in literature [2],[3], less have been performed in the transonic speed range. A gust generator based on oscillating vanes was build for NASA Langley's Transonic Dynamics Tunnel (TDT) [4].
In a new approach the generation of defined and reproducible periodic and transient gusts by an oscillating surface in a transonic wind-tunnel was developed and tested and should be reported in the following. For this existing and newly built test set-ups for a transonic wind tunnel were combined to a new set-up in the test section of the wind tunnel.

2 TEST SET-UP

2.1 Gust Generator

A new set-up was constructed and built, which allows the investigation of two subsequent airfoil-models in the flow of the wind tunnel. The first airfoil is active and should produce a generic gust. This is possible as a continuous sinusoidal wave by pitch oscillations of a rigid 2D airfoil or as transient by an arbitrary wave form, e.g. a 1-cos signal in positive or negative direction. The second profile downstream is flexible and passive and responds only to the unsteady load changes induced by the active moving profile. The arrangement of both models in the measurement section of the DNW-TWG is pictured in figure 1.

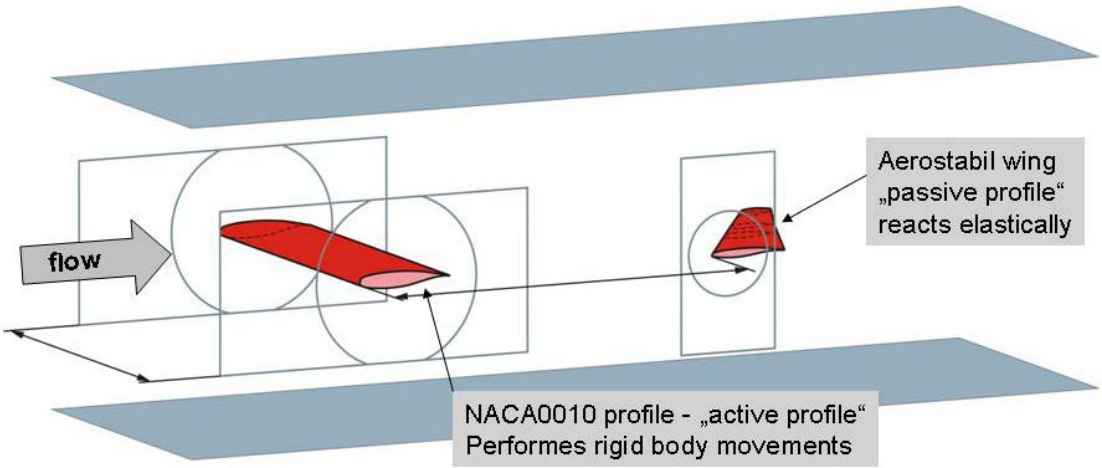

Figure 1: Arrangement of the two airfoil models in the test section of the wind tunnel.

For the generation of the gust, a symmetrical NACA0010 profile was chosen. This allows high flow speeds without transonic effects due to its small thickness. Also wall interference effects are minimized. The 2D airfoil model was build from carbon reinforced fibre and had a span of 997mm and a cord length of 300mm. It was equipped with 64 unsteady Kulite pressure sensors and six accelerometers. The model was mounted to a hydraulic pitch-oscillation test set-up, which is arranged symmetrically outside of each wind-tunnel test-section side wall. Figure 2 shows a sketch of this pitch-oscillation test set-up.

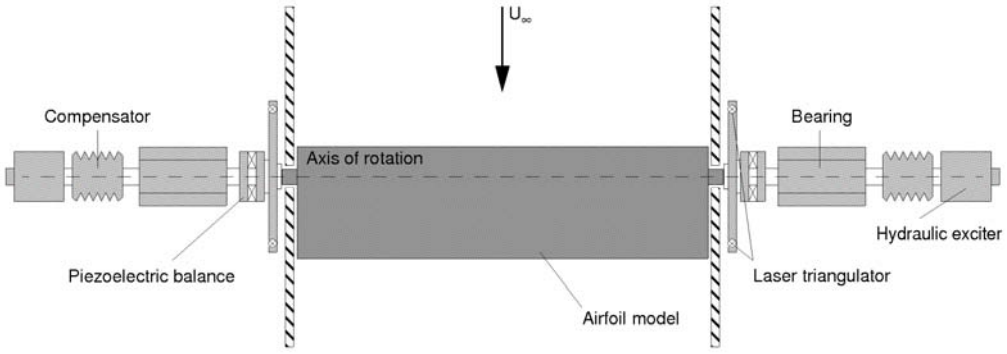

Figure 2: Arrangement of set-up for forced pitch oscillations of the NACA0010 model in the wind tunnel.

The angle of attack of the symmetrically installed model can be varied by ±20° via two hydraulic exciters operated in phase opposition. Forced pitching oscillations up to a frequency of f = 60Hz are possible. The suspension system comprises a compensator, a bearing, a piezoelectric balance and a bar acting as a reference for laser triangulators. By these, the instantaneous angle of attack can be measured by triangulation. Forced harmonic excitation at high pitch amplitudes up to ±20° could be achieved for reduced frequencies up to $\omega^* = 0.1$. Transition was fixed on the upper and lower side at 10% chord length with transition dots of 0.085mm height. For the whole test we defined a right hand coordinate system that originates at the right wind-tunnel wall (looking downstream) at the leading edge of the NACA0010 model at 50% wind-tunnel height. X-direction is downstream, y-direction is in span-wise direction and z- direction is positive in positive lift direction.

2.2 FLIB-Set-Up

For the second airfoil in the wake of the gust generator we decided to use an existing flexible 3d airfoil known as Aerostabil-B model [1]. For the mounting of the model a completely new set-up had to be constructed and built. With this set-up the model can be positioned in vertical direction by ±120mm and rotated to change its steady angle of attack.

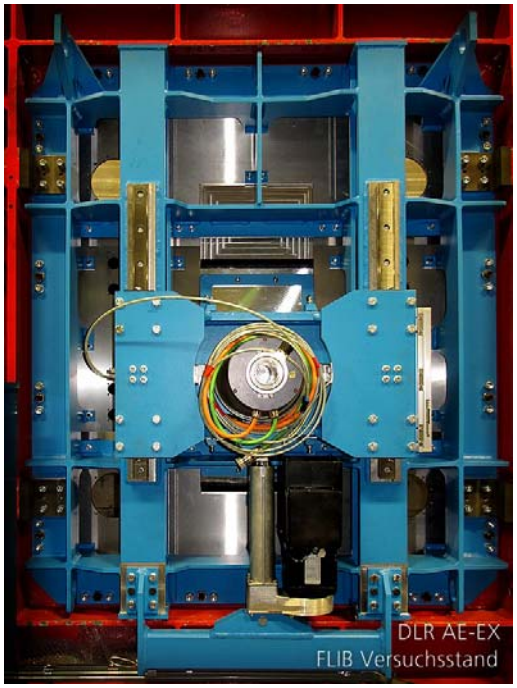

Figure 3 New FLIB set-up (blue) at the side wall of the wind-tunnel test section (red).

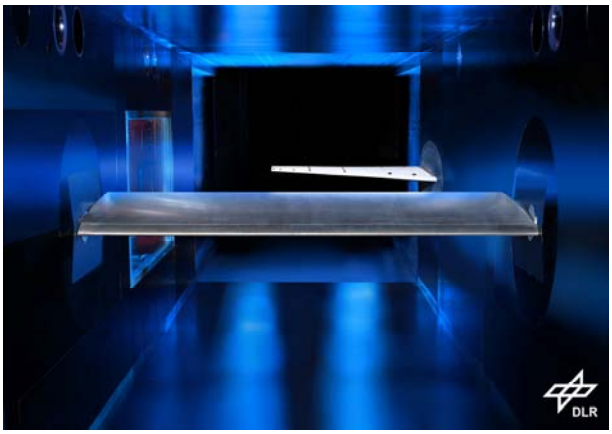

Figure 4: View downstream in the test section with NACA0010 model (foreground) and Aerostabil-B model (background).

2.3 Wind Tunnel

The tests were performed in the Transonic Wind Tunnel Goettingen (TWG), operated by the foundation German-Dutch-Windtunnels (DNW). This is a continuous run facility with a 1m x 1m adaptive test-section. The top and bottom walls of the test section are adapted to the steady flow about the wind-tunnel model. The residual wall interference is minimized by a one step method of wall adaptation based on a Cauchy type integral **[6]** using the top and bottom wall static pressure distributions. The accuracy of the wall pressures is estimated to be ±0.35% with respect to the test stagnation pressure. The displacement thickness of the turbulent wind-tunnel-wall boundary layer is predicted by Head's method **[7]** and is added to the wall shapes; top and bottom wall displacement thicknesses are obtained according to the measured pressure gradients at each wall, while the gradient is neglected for the sidewalls [8]. During the dynamic tests, the wind-tunnel walls were adapted to the steady flow at each mean incidence of the model which was chosen for the following oscillation tests. It was shown in a previous investigation [9] that this minimizes wind-tunnel wall interference effects also during the oscillation tests. The DNW-TWG wind tunnel has the advantage that it covers the whole speed range from Ma=0.300 to Ma=0.850 using the adaptive test section. For a reference chord length of c=0.3m the possible Reynolds number is between 0.5 Mio. and 6 Mio. In figure 5 the whole wind tunnel is depicted schematically.

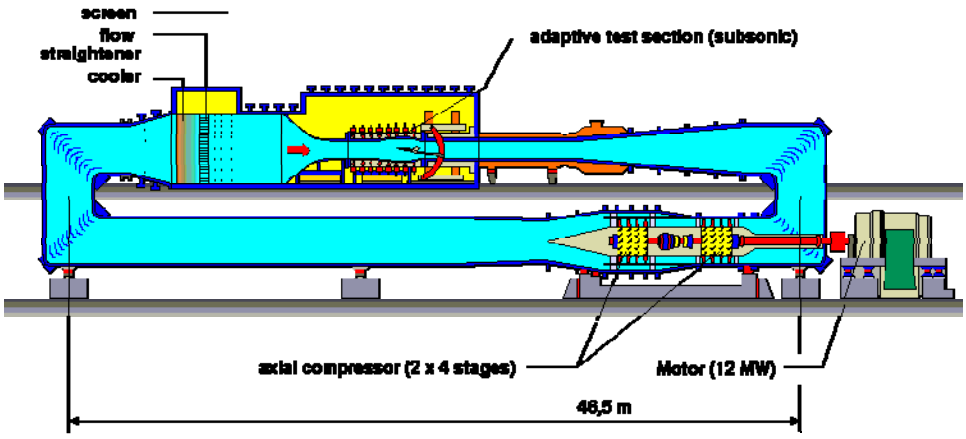

Figure 5: Transonic Wind tunnel Goettingen (DNW-TWG).

2.4 Measurement Techniques

Different measurement techniques were used to measure the aerodynamic and structural parameters during the tests.

2.4.1 Pressure Sensors

For measuring the unsteady pressure distributions on the, surfaces, both wind-tunnel models were equipped with unsteady pressure sensors of type Kulite XCQ-093D. The sensors were mounted right under the pressure taps with special holders. In the NACA0010 model 64 pressure sensors were installed in one mid section. In the Aerostabil-B model 96 pressure sensors were installed in three sections at y/l=32.5%, 44% and 67.5% span-wise direction. The reference side of the differential pressure sensors was connected to the static pressure in the wind tunnel.

2.4.2 Accelerometers

The NACA0010 model was equipped with six accelerometers of type PCB 352C22. They were installed in three sections at y/l=15%, 50% and 85%, in each one sensor close to the leading edge and one close to the trailing edge. By that basic motion, torsion and bending of

the model could be observed. In the Aerostabil-B model, nine accelerometers of the same type were installed as described in [10].

2.4.3 Piezoelectric Balance

The Aerostabil-B model was mounted to a piezoelectric balance. This balance consists of four three-component piezoelectric elements of type Kistler 9047B and 9048B, which are mounted by pre-stressed bolts between two plates. Each element can measure forces in x-, y- and z-direction. In combination of all four elements lift, drag and wall normal forces and roll-, yaw and pitch-moment can be measured. The piezoelectric balance is described in detail in [11].

2.4.4 Data Acquisition System

All unsteady signals were recorded with a data acquisition system that encompasses a 24bit Delta-Sigma A/D converter for each channel. Unsteady signals were: 32 channels of unsteady pressures from the wind-tunnel top and bottom walls, 96 channels of unsteady pressures from the Aerostabil-B model, 64 unsteady pressures from the NACA0010 model, 15 accelerometer signals, 8 balance signals and 4 laser triangulators.
The system is capable of acquiring data with a maximum sample rate of 204.8kHz per channel. For the present test a sample rate of 128 times the excitation frequency was used. Steady mean data from the wind tunnel, like total pressure, static pressure, static temperature, Mach number, steady wall pressures and wall position are transferred by file to the data acquisition system and saved together with the unsteady data. For the optical position measurement a special system was used that was time synchronized with the data acquisition system and is described in the next section.

2.4.5 Optical Position Measurement System PicColor

As the answer of the second airfoil was one of the key information for this test, an optical position measurement system was used to measure its deflection. This consist of two powerful LED illuminations, two Microtron 1310 CCD video cameras, two frame grabber, a fast PC and special “PicColor” software for tracking markers. The system in its present configuration is capable of tracking up to 24 markers at a maximum frequency of 500Hz. With that frequency, for each marker its actual x-, y- and z-position in a calibrated reference coordinate system are written to disc. The accuracy of the system is depending on the optical arrangement and was estimated in this test to be better than 0,1mm for the z-component [12].

Figure 6: Aerostabil-B model with 24 PicColor markers in seven sections on its upper surface.

2.5 Test Programme

As the behaviour of the two models in the wind tunnel as a forced response system was totally unknown, it was decided to excite the second model around its lowest eigen-frequency. This was known from former tests [10] to be a first bending at about 37.8 Hz without aerodynamic loads. To have simple flow conditions at the exciting airfoil, a shock free condition at Ma = 0.750 and an excitation amplitude of $\hat{\alpha} = 0.7°$ around a mean angle of attack of $\alpha = 0°$ was chosen. As a second test case Ma = 0.800 and an amplitude of $\hat{\alpha} = 0.5°$ at an angle of attack of $\alpha = 2°$ was selected as a case close to a shock-buffet condition. As reference a subsonic case at Ma = 0.600 was chosen. For these three test cases, harmonic oscillations of the gust generator were investigated for a position of the second airfoil at the same height directly in the wake of the first airfoil. Furthermore the elevation of the second airfoil was varied between -80mm and +80mm.
For the three Mach numbers also transient excitation by a 1-cos gust was tested, too. These were the objectives of the forced response experiment. But first the wake itself was to be investigated.

2.6 Investigation of the Wake by PIV

In a first experiment in 2009 only the active NACA0010 model was installed in the wind-tunnel. Aim of this experiment was to characterize the unsteady wake of the continuously oscillating airfoil by Particle Image Velocimetry (PIV). PIV measurements were taken in a section at the location where the second airfoil model was to be mounted in the second test. The location in the wind-tunnel test section can be seen on figure 7. The observation field was 300mm wide and 200mm high.

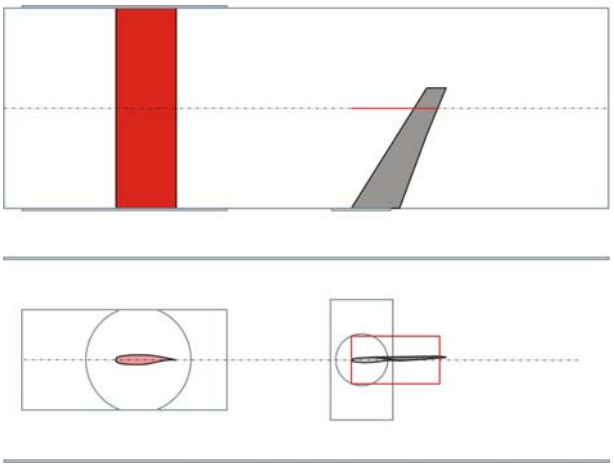

Figure 7: Location of PIV observation window in flow direction (red). Upper: View from top. Lower: Side view.

By this it was possible to characterize the source of excitation. PIV images where taken phase locked for 36 phase angles relative to the oscillating airfoil. For each phase angle 500 instantaneous pictures where taken. In figure 8 we show the vorticity for such a single picture and the x-velocity component as a mean of 500 pictures for a certain phase angle.

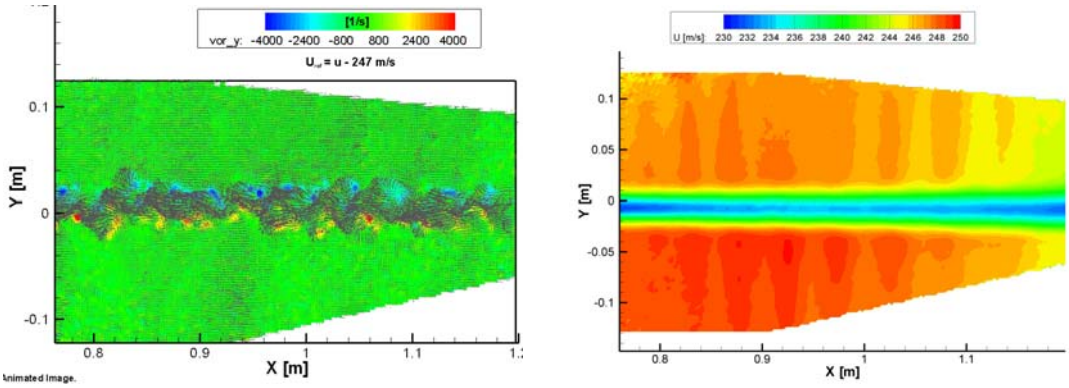

Figure 8: Left: Single PIV image for one phase angle in configuration 1. Right: Mean flow velocity calculated from 500 PIV images

3 PRE-INVESTIGATION FOR THE GENERIC GUST GENERATOR EXPERIMENT BY COUPLED CFD-CSM SIMULATIONS

In order to support the preparation of the wind-tunnel experiment and to estimate, whether the generic gust generator will be able to produce significant vortices which in turn excite the elastic wing (Aerostabil-B model), a series of coupled simulations were performed in advance. The simulations should reveal the strength of the expected unsteady forces and the response amplitudes of the elastic wing. For this purpose different steady and unsteady simulations by using an in-house developed PYTHON process chain for fluid-structure interaction [13] have been carried out. In the following section, a brief mathematical description of the coupling method and the used numerical models will be shown.

3.1 Numerical approach for coupled simulations

The used coupling approach for the performed simulations is based on a weak code coupling for fluid-structure interaction. In this coupling procedure for the calculation of the aerodynamic forces the DLR-TAU Code has been used [14]. For the prediction of the static and dynamic elastic deformations, an improved NASTRAN finite element shell model of the Aerostabil-B model was used. All presented coupling simulations were performed by using a modal fluid-structure coupling approach. In the next section this approach will be described shortly.

3.1.1 Steady simulations for aeroelastic equilibrium

The coupling of aerodynamics, usually represented by a CFD model, and structural dynamics, represented by a FE model, is accomplished via the so called *weak coupling* strategy. At this method the flow solver and the structural solver each integrate their respective governing equations separately. Boundary conditions are exchanged in each iteration step via an interpolation method based on scattered data which becomes necessary due to the different model discretisation on their common surfaces. The data exchange is carried out until a specified convergence criterion is reached. The chosen convergence criterion can be the minimum of the differences between the last and the actual maximum displacement of a certain point of the structure. The data are exchanged between the flow solver and the structural solver by spatial interpolation. For any steady and unsteady coupled aeroelastic simulation presented in this paper, the below described modal approach is used. The governing equation for a linear elastic structure in physical coordinates can be written as:

$$Ku = f \tag{1}$$

Herein K is the stiffness matrix, f the vector of the external forces and u the corresponding displacement vector. In the modal approach the structural elasticity is introduced from a modal decomposition of the discrete finite element model, thus leading to a linearly approximated elastic model based on a reduced number of modal degrees of freedom. With the mass-orthogonally scaled modeshapes Φ_s, and the generalized coordinates q the physical displacements can be expressed as:

$$u_s = \Phi_s q \tag{2}$$

Equation (1) can then be written as:

$$K\Phi_s q = f_s \tag{3}$$

Multiplying this equation again with the transposed modal basis Φ_s^T leads to:

$$\Phi_s^T K \Phi_s \, q = \Phi_s^T f_s \tag{4}$$

Due to the mass-orthogonally scaled eigenmodes, the expression $\Phi_s^T K \Phi_s = \mathrm{diag}\left(\varpi^2\right) = \Omega$, equation (4) becomes:

$$\Omega q = \Phi_s^T f_s \tag{5}$$

Assuming that each eigenmode of the structure can be interpolated to the aerodynamic surface via an adequate interpolation method, the interpolated mode shapes of each eigenvalue on the aerodynamic surface can expressed by $\Phi_a = H\Phi_s$, respectively $\Phi_a^T = \Phi_s^T H^T = \left(H\Phi_s\right)^T$. The linear equation (5) then gets the form

$$\begin{aligned} q &= \Omega^{-1}\Phi_s^T f_s \\ &= \Omega^{-1}\left(H\Phi_s\right)^T f_a \\ &= \Omega^{-1}\Phi_a^T f_a \end{aligned} \tag{6}$$

where f_a now are the aerodynamic forces acting on the aerodynamic surface and obtained directly from the CFD calculation. The eigenvalues occur in the modal stiffness matrix $\Omega = \mathrm{diag}\left(\omega_1^2, \ldots, \omega_n^2\right)$. The right hand side of equation (6) shows the equivalence of the explicit back transfer of the aerodynamic forces and a following projection onto the structural eigenmodes to the direct projection of aerodynamic forces onto the individual mode shapes on the aerodynamic surface. The physical deformations of the aerodynamic surface have to be subsequently determined by:

$$u_a = \Phi_a q \tag{7}$$

A reasonable number of structural modes must be chosen to represent the dynamic and static behaviour appropriately. The structural eigenmodes need to be interpolated on the aerodynamic mesh only once during a pre-processing step.

3.1.2 Unsteady simulations for the gust response analysis

For unsteady simulations the governing equation of motion in physical coordinates is:

$$M\ddot{u}(t) + D\dot{u}(t) + Ku(t) = f(t) \tag{8}$$

The transformation of this equation into generalized coordinates and normalization of the mode shapes in this way that the generalized mass matrix becomes the unit matrix as well as neglecting the structural damping leads to:

$$I\ddot{q}(t) + \Omega q(t) = \Phi_s^T f_s(t) \tag{9}$$

In this equation the mode shape matrix describes the behaviour for the structural degrees of freedom and the forces act on the structural node points. In order to get the aerodynamic forces instead of the structural forces, we use a scattered data interpolation approach [15],[16] by introducing the coupling matrix H as a linear combination for the structural deflections:

$$u_a = Hu_s \tag{10}$$

It can be shown that the aerodynamic forces can be transformed by using the transposed interpolation matrix H in a conservative way, which means that the global equilibrium for forces and moments is ensured and the virtual work performed on both sides is the same. Over the principal of the virtual work we get the linear coherency:

$$f_s = H^T f_a \tag{11}$$

By inserting this approach into the generalised equation of motion finally follows:

$$\begin{aligned} I\ddot{q}(t) + \Omega q(t) &= \Phi_s^T H^T f_a(t) \\ &= (H\Phi_s)^T f_a(t) \\ &= \Phi_a^T f_a(t) \end{aligned} \tag{12}$$

In this equation Φ_a are the interpolated structural mode shapes on the aerodynamic surface points. In order to solve this equation for each physical time step an implicit Newmark integration schema and a conventional serial staggered algorithm with a predictor and corrector step for the aerodynamic forces is used. The procedure for the data exchange in each time step is schematically shown in figure 9. For the mesh deformation after each coupling step we use an advancing front algorithm which has been described in [17]. First unsteady simulation results using this approach have been presented in [18].

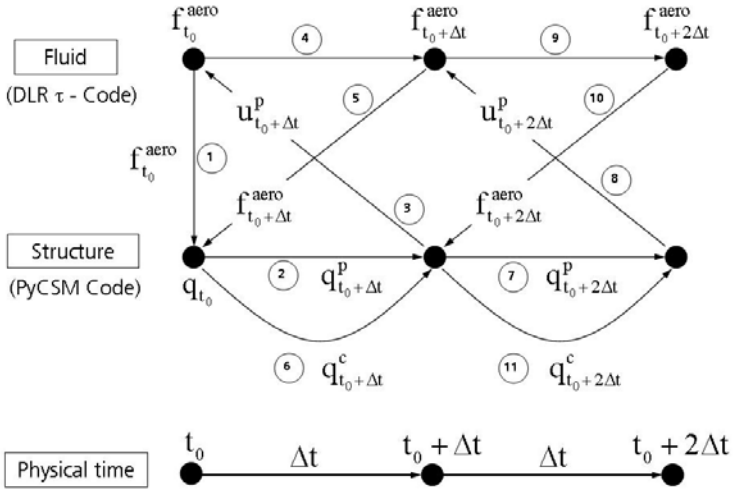

Figure 9: Coupling procedure for unsteady simulations.

3.2 Used numerical models

In the following the used numerical models will be described. For the elastic behaviour of the passive wing, a finite element model was generated. The active wing (NACA0010 model) is performing only forced and well-ordered rigid body motions. Furthermore it is assumed that this model will not produce significant elastic deformations under load. Hence this model has no underlying finite element model. For aerodynamic model discretisation both profiles were meshed together by using the CENTAUR mesh generator [19].

3.2.1 Structure mechanics model

The used structure model is an improved finite element model of the elastic Aerostabil-B model from [10]. This new model has been introduced and explained for the first time in [20]. Due to the fact that the elastic behaviour of this wing was more complex than a simple Bernoulli beam model can describe under the assumption of complete cross section preservation, a more complex finite element model has been constructed by using an in-house developed model generator ModGen [21] and Nastran. In figure 10 a selected number of mode shapes of the used shell model are presented. One can see that the cross section is deforming significantly, especially at the trailing edge. These deformations have a large influence on the aerodynamic pressure distribution due to the elastic deflections of the wing. Compared with experimental determined mode shapes the elastic behaviour is now much better than with the old beam model.

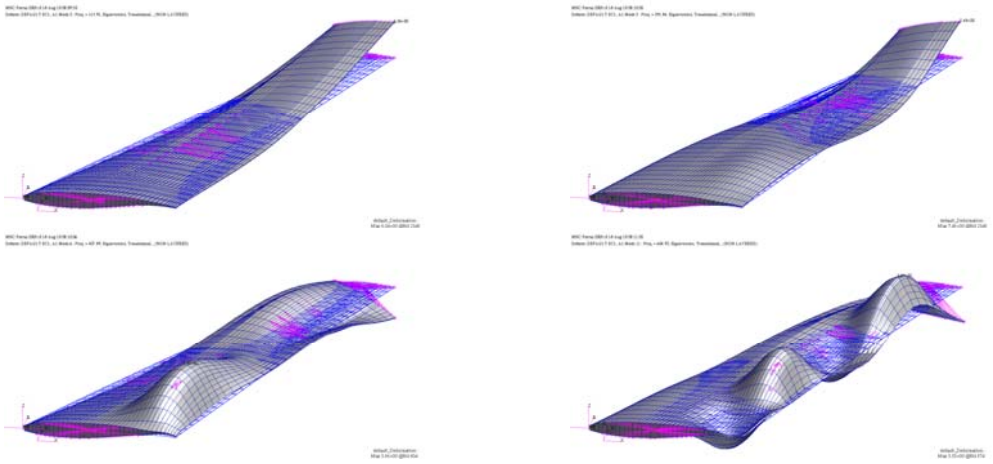

Figure 10: Finite element model of the Aerostabil wing – mode shapes 2, 5, 6 and 11

3.2.2 Aerodynamic model

For the aerodynamic mesh generation, the CENTAUR software has been used. The geometric descriptions of both models were combined in one and meshed with several mesh refinement regimes for the surface discretisation. For a better transport of the unsteady wake a mesh refinement regime around the profiles has been generated as a geometric source, see figure 11. The side walls are modelled with symmetry boundary conditions. The wall effects of the upper and lower wind tunnel walls have been neglected for this preliminary investigation. Therefore the upper and lower walls were described as farfield boundary conditions. The entire mesh has no boundary layer, because the frictionless Euler equations are solved for all preliminary calculations. This has been done to get results in short time and to stay conservative regarding the aerodynamic forces. Due to the neglect of friction effects the aerodynamic forces are higher and thereby the expected elastic deformations as well. Thus it can be ensured that maximum stresses and strains, as a result of large predicted deformations of the elastic wing, will probably be overrated.

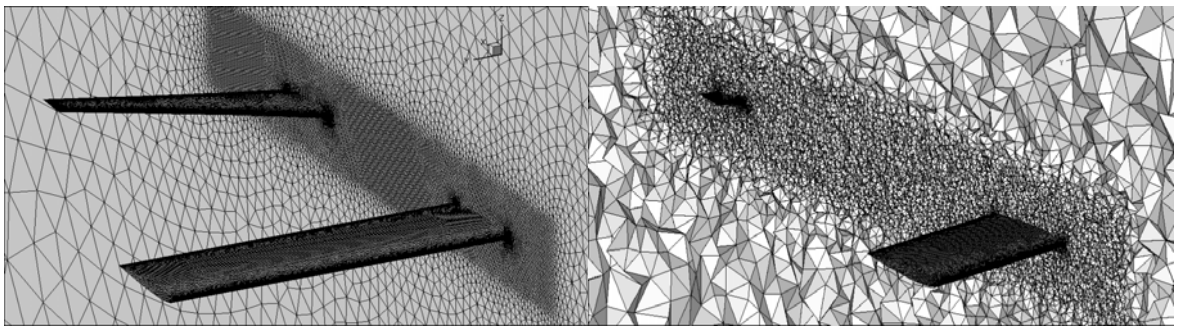

Figure 11: Aerodynamic mesh for steady and unsteady simulations of the generic gust generator experiment.

In table 1 the dimensions of the used mesh for the Euler calculations are listed.

Number of nodes	Number of total cells	Number of surface cells
~ 700000	~ 3.9 Million	~ 101000

Table 1: Mesh dimensions for the used CFD mesh.

4 RESULTS

For first investigation regarding the steady and unsteady behaviour of the elastic wing model, different simulations with the models described above have been performed. First the characteristic flow parameters for the simulations had to be defined. Thereby it should be ensured that no separated flow occurs. Possible unsteady effects, which could appear yet in the steady calculations, should be induced at most by the wake of the leading profile. Second a complex aerodynamic flow with shocks that could occur already at the leading profile should be excluded a priori. For these preliminary investigations, the superior aim was at first to start at less complex flow conditions to get stable numerical simulations and to get results for the complex time domain simulations in adequate time. In table 2 the used flow parameters for the steady simulation are listed.

Description	Value
Mach number [-]	0.75
Reference density [kg/m³]	0.523
Reference temperature [K]	275
AoA of NACA0010 [deg]	0.0
AoA of Aerostabil wing [deg]	0.0

Table 2: Reference flow parameters for steady and unsteady coupled simulations.

The steady aeroelastic equilibrium state for these flow conditions was the starting point for all upcoming unsteady simulations.

4.1 Steady results

In this section the steady results like pressure coefficients on both profiles and the elastic deformations of the passive wing will be shown and compared with the experimental results. As mentioned before all numerical calculations have been performed in advance without any knowledge of the experimental behaviour.

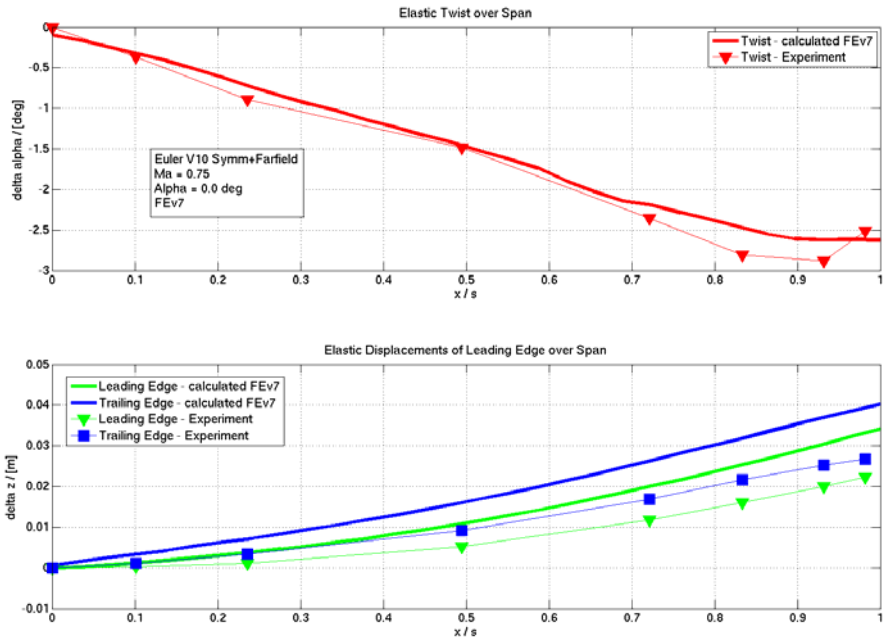

Figure 12: Experimental versus calculated elastic deformations of the Aerostabil-B model in aeroelastic equilibrium state. **Top:** twist over scaled span. **Bottom:** bending of the leading and trailing edge.

In figure 12 the calculated and the experimentally determined deformations like the bending of the leading and the trailing edge as well as the elastic changing of the local angles of attack is depicted. It is recognizable that the calculated bending is much higher than the experimental one obtained by the PicColor system. In contrast to this, the elastic twist distribution fits quite well with the values from the experiment. As the local angle of attack is much more important for the pressure distribution than the local bending, the pressure coefficients shown in figure 13 match quite well. The c_p-values are shown for three measurement sections at y=0.195m, 0.264m and 0.405m. Due to the neglected viscous effects by the frictionless flow conditions, the calculated load distribution especially on the top of the wing has been overrated.

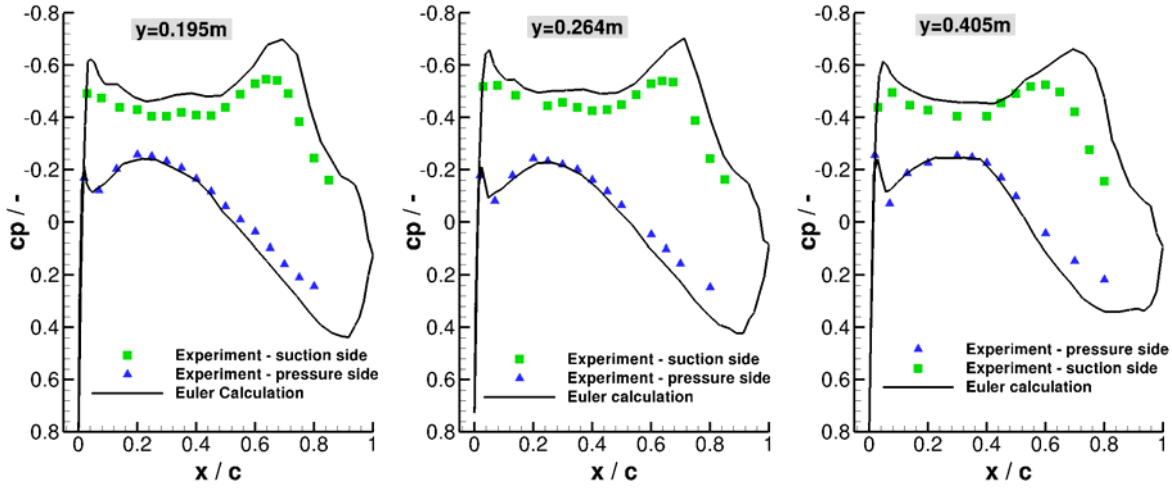

Figure 13: Experimental measured versus calculated c_p distribution for three sections (y=0.196/0.264/ 0.405m) of the elastic Aerostabil-B wing in aeroelastic equilibrium state for the reference case.

In figure 14 the pressure distribution at the leading NACA0010 model for the mid-span section at y=0.5m is depicted. The comparison between experiment and simulation shows a quite good agreement. Due to the neglected friction, the calculated pressure in the first 30% of the chord is again overrated.

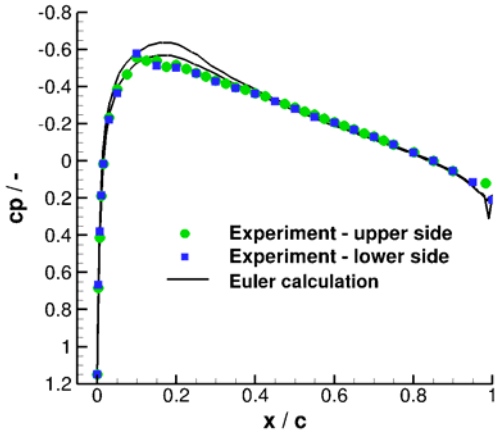

Figure 14: Experimentally measured versus calculated c_p distributions of the NACA0010 model for the reference case at mid-span section y=0.5m.

Figure 15 shows the complete setup of the generic gust generator experiment in the simulation. Coloured are the pressure distributions on both profiles as well as in the symmetry plane for the static aeroelastic equilibrium state.

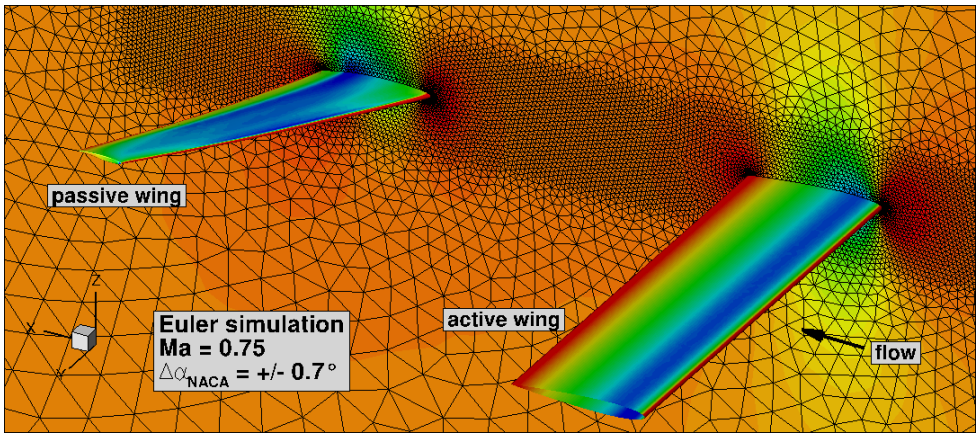

Figure 15: C_p distributions of both profiles after a steady coupled simulation in steady aeroelastic equilibrium state.

This steady aeroelastic equilibrium state is the initial condition for all upcoming unsteady simulations, where variations of the amplitudes and the excitation frequency of the NACA0010 model have been carried out. For the variations of the vertical position of the passive wing, further calculations had to be done.

4.2 Unsteady Results

In order to get first information about the behaviour of the elastic wing during the experiment, a number of parameter variations for the numerical simulations have been determined. The simulations regarding these parameter variations should give advice of the maximum possible excitation amplitude that could be run for the NACA0010 model and the thereby caused response characteristic of the elastic Aerostabil-B model. Furthermore, a frequency variation should reveal the resonance frequency of the Aerostabil-B model under aerodynamic loads and the thereby occurring maximum amplitude. A variation of the vertical position of the elastic wing should give answer, whether it is possible to position the elastic wing outside of the unsteady wake and thereby reduce the amplitudes and hence the unsteady loads of the wing. The parameter variations, which have been used for the simulations, are listed in table 3. The reference case has the blue coloured parameter settings. The parameters, which then have been changed, are listed in red. The frequency of the reference case setting is the first frequency of the elastic wing of the finite element model. At zero vertical position, both models lie in the same x-y-plane. In the following all calculated amplitudes are zero to peak values. The zero state means thereby the mean value of the unsteady elastic deformation.

Calculations	Δα (NACA0010)	Frequency f (NACA0010)	Vertical Position Δz (Aerostabil-B)	Angle of attack α_0 (Aerostabil-B)
Reference case	±0.7°	37.89 Hz	0.0 mm	0.0°
Amplitude variation	±0.4°, 1.0°, 1.3°	37.89 Hz	0.0 mm	0.0°
Frequency variation	±0.7°	1, 10, 20, 30, 35, 41, 43, 45, 50 Hz	0.0 mm	0.0°
Variation of the vertical position	±0.7°	37.89 Hz	±20, 40, 80 mm	0.0°

Table 3: Variations of different parameters for all unsteady coupled simulations of the generic gust generator experiment.

Before starting with the numerical investigation by coupled unsteady simulations for the reference case as defined in table 3, a convergence study regarding the maximum number of time steps per period, which are necessary, has been carried out. The results are shown in figure 16. Depicted are the maximum occurring amplitudes at the wing tip of the elastic wing against the used number of time steps per period. It can be pointed out, that after a number of 100 time steps per period, the results are converged. Hence for all simulations this number of time steps has been used.

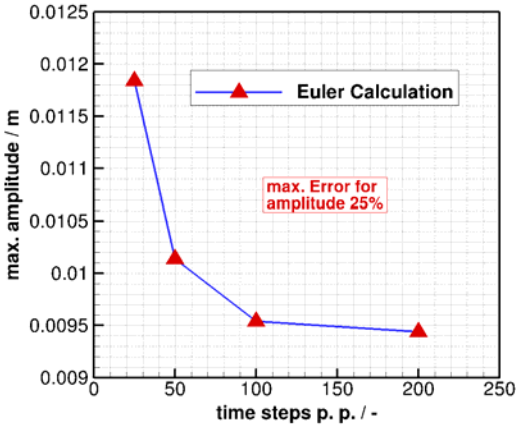

Figure 16: Development of the maximum amplitude of the Aerostabil-B model as a function of the number of time steps per period for the dual time stepping scheme.

Then the elastic forced response behaviour of the passive wing by changing the height of the excitation amplitude has been investigated. In figure 17 the maximum deformation of the wing tip of the Aerostabil-B model is depicted as a function of the excitation amplitude in degrees. It turned out that the response of the wing is linear dependent of the excitation amplitude in the investigated range up to an amplitude of 1.3°.

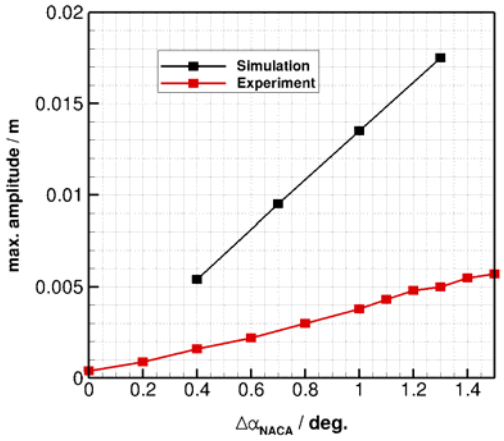

Figure 17: Comparison between experiment and calculation for the development of the maximum amplitude of the passive Aerostabil-B model as a function of the excitation amplitude of the leading NACA0010 model.

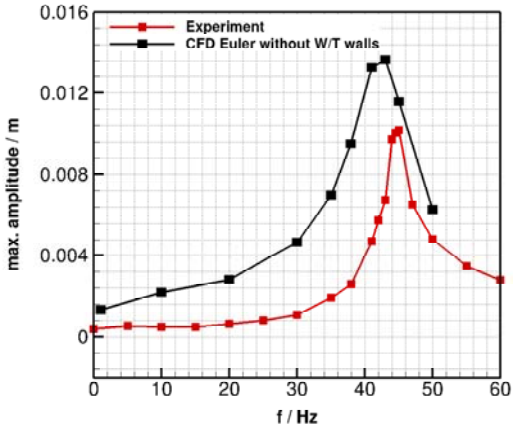

Figure 18: Comparison between experiment and calculation for the development of the maximum Amplitude of the passive Aerostabil-B model as a function of the excitation frequency of the leading NACA0010 model.

Next the frequency variation was investigated. Thereby the dependency of the elastic behaviour of the passive wing by changing the excitation frequency was simulated for the reference case, see table 3. In figure 18 the results are depicted and compared to the experiment. Shown are the maximum amplitudes that could be reached by variation of the

excitation frequency. The maximum amplitude in the numerical simulation has occurred at 43 Hz and got a height of approximately 14mm. The resonance frequency under flow condition has increased around 14% against the first eigenfrequency of the elastic wing without flow. Visible amplitudes in the experiment should thereby first occur at frequencies above 30 Hz. Because in all calculations viscous effects have been neglected, the acting forces hence are much higher than in the experiment. As all calculated amplitudes were overrated, the safety of the elastic model in the experiment was given.
The last investigation referred to the influence of the vertical position of the passive wing on its maximum occurring amplitude. Therefore the position of the Aerostabil-B model has been varied in z-direction between $\Delta z=\pm 80$mm. In the left picture of figure 19 a new generated computational fluid dynamics mesh for this purpose with a variation of $\Delta z=+40$mm is depicted. The influences of the vertical positions regarding the amplitudes are shown in the right picture of figure 19. The calculations have been performed for the reference case flow conditions defined in table 3. It can be seen that the investigated vertical position has a significant influence on the elastic behaviour. The loss of the amplitude at position $\Delta z=-80$mm is about 20% in proportion to the maximum occurring amplitude at position $\Delta z=+20$mm.

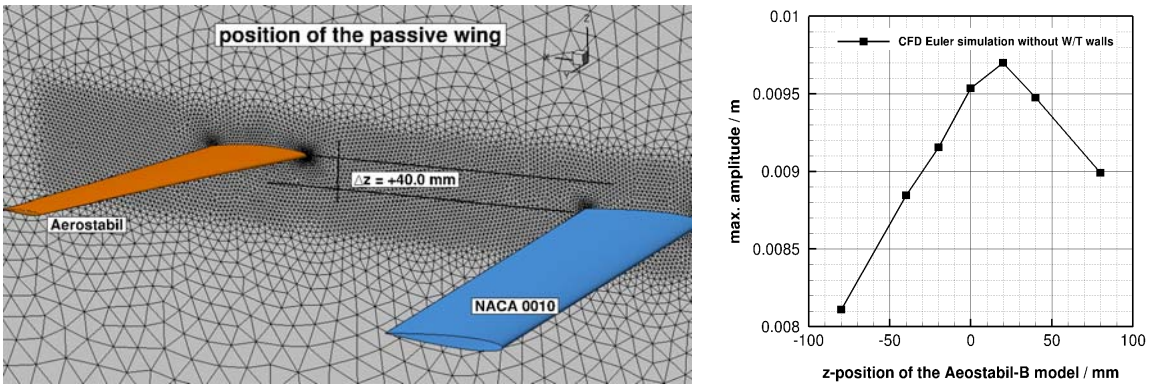

Figure 19: **Left:** Variation of the vertical position of the passive Aerostabil-B model outside of the x-y-plane of the wake of the leading profile (NACA0010). **Right:** Development of the maximum amplitude of the passive Aerostabil-B model as a function of its vertical position.

For all calculations we have to take into account that the influences of the wind-tunnel walls have been neglected. Therefore it is likely that the amplitudes in the experiment will differ from this pre-calculation.
One further simulation has been done to examine the plausibility of the simulation results by defining a forced response simulation where the global movement of the elastic model should be clear. Thus the unsteady simulation has been started from aeroelastic equilibrium state without any excitation for the time of one period. After this the excitation has been started and performed for 12 periods and than abruptly finished. During the first period before starting with the movement of the NACA0010 model, no elastic deformations should be seen and the integral forces on the elastic wing should not change. Then, after starting with the movement of the active wing, it should take a short time until the unsteady wake impacts the passive wing and the excitation starts. When the gust generator then stops its motion, it should once again give a time delay until the unsteady wake vanishes and the elastic wing turns back in its initial condition, the steady aeroelastic equilibrium state.
The results for this kind of simulation are shown in figure 20. At the top of the figure, the changing of the angle of attack for the active wing over time is depicted. The middle graphics shows the elastic deflection of the wing tip of the passive wing, and in the bottom graphic the induced unsteady forces on the passive wing are pictured. Aside from the size of

the values, the simulation showed the expected behaviour. The time delays are recognizable before starting the movement of the active wing regarding the reactions of the elastic profile as well as the changes in the unsteady forces acting on the elastic wing. After the movement has finished, the elastic system turns back in its initial conditions.

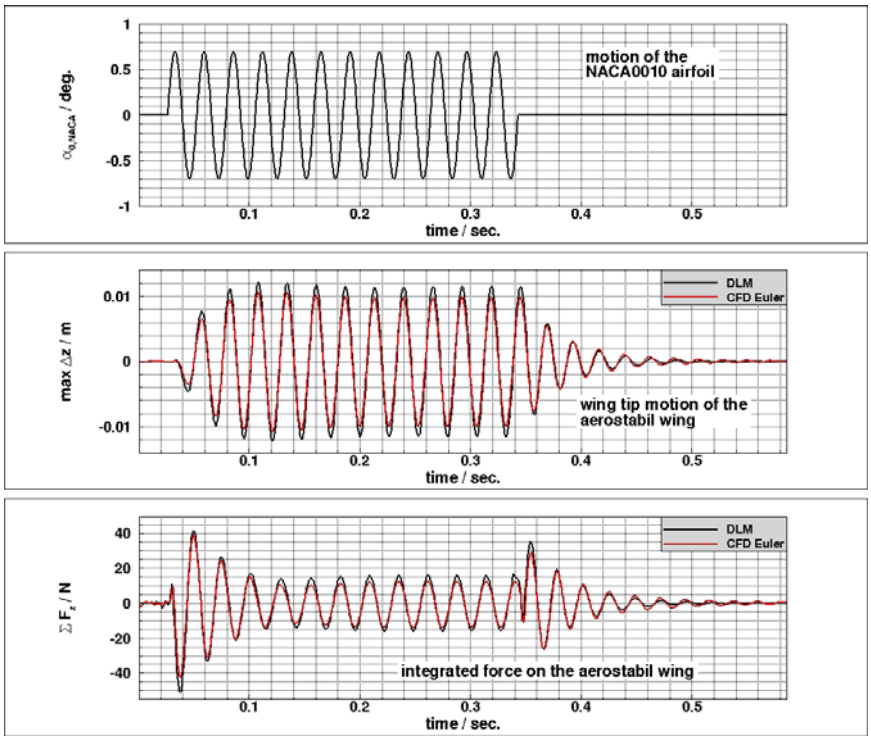

Figure 20: Time progress of the amplitude for the active wing (upper), the wing tip displacement of the passive wing (middle) and the induced forces on the passive wing (lower) during a coupled simulation of the generic gust in comparison to Doublet Lattice Aerodynamics calculation.

Furthermore this simulation has also been performed with a fast doublet lattice method using the commercial software MSC NASTRAN. The comparisons of both results are also depicted in figure 20 and show a very good agreement for the elastic deformations as well as for the induced unsteady loads on the passive wing. This comparison ensured that no mistake during the complex model setup for the coupled simulation has been done and validated hence the whole in-house coupling process chain PyCSM.
To get an impression of the whole simulation, in figure 21 the pictures of two time steps in the last period are shown. Depicted is the strength of the vorticity around the y-axis in two different sections. One in the symmetry plane and one in the x-z-plane at y=0.55m.

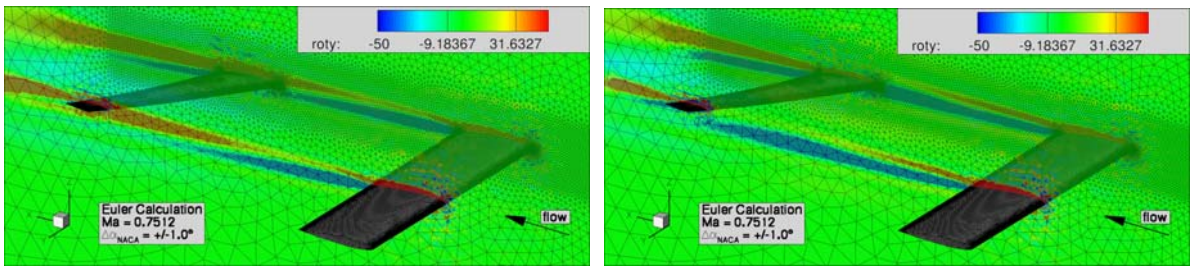

Figure 21: Simulation of a gust using a rigid moving NACA0010 model and an elastic reacting wing model (Aerostabil-B model).

In comparison to the calculation shown in figure 20, a 1-cos gust was investigated in the experiment. For this, the active NACA0010 model performed a single 1-cos oscillation between 0° and 7° with a frequency of 10Hz as shown in figure 22, upper row. The answer, e.g. the wing-tip deflection of the Aerostabil-B model, is low but significant. In a follow-up experiment this could be tested also with an excitation frequency closer to the resonance frequency of 43Hz to get higher response amplitudes.

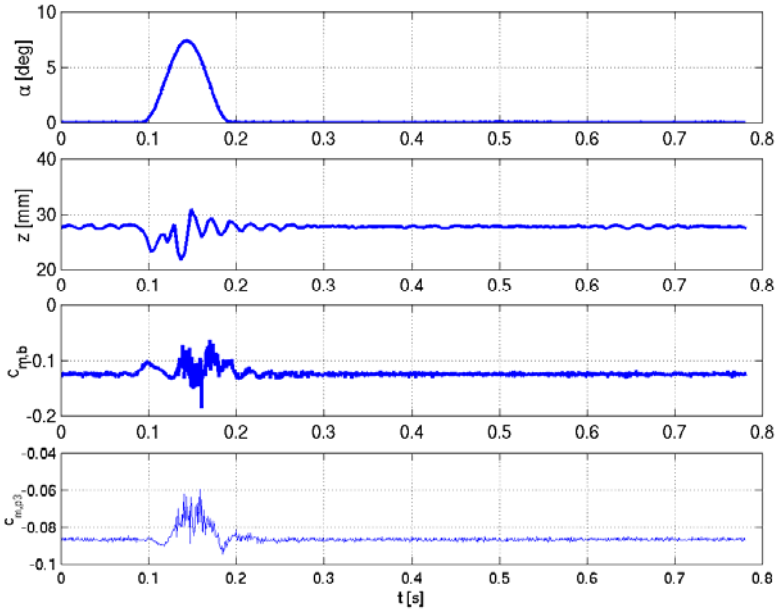

Figure 22: Simulation of a 1-cos gust in the wind-tunnel experiment. Top row: Motion of the NACA0010 model. Second row: Wing-tip deflection of the Aerostabil-B model measured by PicColor. Third row: Global moment coefficient measured by the piezoelectric balance. Bottom row: Local moment coefficient at the pressure section y/l=67.5% of the Aerostabil-B model.

5 SUMMARY AND CONCLUSIONS

In two wind-tunnel test campaigns in 2009 and 2010 in the DNW-TWG transonic wind-tunnel facility a new set-up for simulating unsteady flow fields and transient gusts was tested. The new set-up comprises two individual mounting points for wind-tunnel models, where the first has the possibility to mount 2D models and perform forced pitch oscillations and transient angle of attack variations. The second set-up downstream of the first is capable of mounting a 3D model, e.g. a flexible swept wing and change the angle of attack and vertical position of this model.

In the first test, the unsteady flow field of the gust generator was investigated by PIV. In the second test variations of Mach number, excitation frequency and amplitude as well as 1-cos gust excitation were investigated on the flexible Aerostabil-B model. For the preparation of the experiment, extensive numerical simulations have been carried out in advance. Therefore model simplifications inside the simulation models have been done in order to get first information about the behaviour of this complex experiment. Especially simplifications regarding the flow conditions like neglecting viscous effects of the flow and ignoring wind-tunnel wall effects have to be mentioned here. For further investigation and simulations these effects should be taken into account. Hence, in the future calculations using improved CFD meshes for better numerical models have to be generated. Especially the influence of the wind-tunnel walls regarding the unsteady behaviour of the elastic wing shall be investigated soon. Also improvements of the finite element model for the well known

complex elastic behaviour of the real wing model could finally improve the results obtained up to now.
With a further updated structural model (by static test in the wind-tunnel mounting) sophisticated CFD calculations with higher order methods like DLR TAU code should be validated in the near future. Different numerical codes should be compared.
For the approval of aircraft, the 1-cos simulation in the wind-tunnel may lead to greater confidence in numerical simulation for this task.
After the qualification of this new innovative set-up in the wind-tunnel further application can be imagined like test of gust control systems for load alleviation or helicopter tip vortex interaction.

6 AKNOWLEDGEMENTS

This work was founded by DLR programmatic research in a project called “iGREEN”. The authors would like to thank Mr. J. Berold for thorough preparation of the wind-tunnel models, Mr. Th. Buete being responsible for the operation of the two test set-ups, Mrs. A. Hebler and Mr. J. Nuhn for thorough preparation and conduction of the test and acquisition of the data, Mr. A. Schroeder and Mr. R. Geisler for the PIV measurements, and the DNW team for their support and operation of the wind tunnel.

7 REFERENCES

[1] HOBLIT F.M., *Gust Loads on Aircraft: Concepts and Applications*, AIAA Education Series, Washington, 1988.

[2] AMIRYANTS G.A., ET AL., *Design, Manufacture and Wind Tunnel Testing of the Multi-Functional European Research Aeroelastic Model (EuRAM),* European Conference for Aerospace Sciences (EUCASS) Moscow, Russia, July 2005.

[3] MOULIN B., KARPEL M., *Gust Loads Alleviation Using Special Control Surfaces*, Journal of Aircraft, Vol. 44, No. 1, February 2007.

[4] TANG D.M., CIZMAS P., DOWELL E. H., *Experiments and Analysis for a Gust Generator in a Wind Tunnel*, Journal of Aircraft, Vol. 33, No. 1, pp. 139-148, 1996.

[5] GERHOLD T., ET AL., *Calculation of Complex Three-Dimensional Configurations Employing the DLR-TAU Code*, 35th Aerospace and Science Meeting and Exhibit, Reno, AIAA-97-0167, January 1997.

[6] WEDEMEYER, E., TAYLOR, N. J., AND HOLST, H., *Adaptive Wall Techniques*, AG 336, AGARD, 1998.

[7] CEBECI, T., BRADSHAW, P., *Momentum Transfer in Boundary Layers*, McGraw-Hill, New York, 1979.

[8] JACOBS, M., *Treatment of the Wall Boundary Layer in the Wall Adaptation Procedure and Steady Wall Adaptation for Dynamic Tests*, private communication, DNW BU GuK,Goettingen, 2002.

[9] GEIßLER W., DIETZ G., MAI H., *Dynamic Stall on a Supercritical Airfoil,* 29th European Rotorcraft Forum, 16.–18. September 2003, Friedrichshafen, Germany, 2003.

[10] DIETZ G., SCHEWE G., KIEßLING F., SINAPIUS M., *Limit-Cycle Oscillation Experiment at a Transport Aircraft Wing Model*, Proceedings of the International Forum on Aeroelasticity and Structural Dynamics, IFASD 2003, Amsterdam, the Netherlands, 2003.

[11] SCHEWE G., *Force measurements in aeroelasticity using piezoelectric multicomponent transducers,* International Forum on Aeroelasticity and Structural Dynamics, Aachen, June 3–6, DGLR Report 91-06, 1991.

[12] SICILIA G., *Optical Deformation Measurements of the Aerostabil-B Wing during the iGREEN FLIB-2 Wind-Tunnel Experiment using PicColor*, DLR IB 232 – 2011 C 08, 2011.

[13] NEUMANN J., *PyCSM – Python Computational Fluid Dynamics and Computational Structure Mechanics Coupling System,* Software Documentation and Technical Report, Institute of Aeroelasticity, State: November 2010, Goettingen.

[14] GERHOLD T., GALLE M., FRIEDRICH O., EVANS J., *Calculation of Complex Three-Dimensional Configurations Employing the DLR-TAU Code*, AIAA Paper 97-0167.

[15] BECKERT A., WENDLAND H., *Multivariate Interpolation for Fluid-Structure-Interaction Problems using Radial Basis Functions*. Aerospace Science and Technology, Art. No. 5125.

[16] NEUMANN J., *Identifikation radialer Basisfunktionen zur räumlichen Strömungs-Struktur-Kopplung unter Berücksichtigung des Interpolations- und des Lasttransformationsfehlers*, DLR IB 232 – 2008 J 01, 2008.

[17] GERHOLD T., NEUMANN J., *The parallel mesh deformation of the DLR TAU-Code.* 15. DGLR-Fach-Symposium der STAB, Nr. 2006-11-29-2006-12-01, Darmstadt, Germany.

[18] NEUMANN J., RITTER, M., *Steady and Unsteady Aeroelastic Simulations of the HIRENASD Wind Tunnel Experiment,* IFASD - International Forum on Aeroelasticity and Structural Dynamics, 21 - 24 June 2009, Seattle, WA, USA.

[19] CentaurSoft, CENTAUR, http://www.centaursoft.com.

[20] STICKAN B., DILLINGER J., *Coupled CFD-CSM Simulations of the Aerostabil Windtunnel Experiments, considering Sophisticated Structural Modelling*. In Proceedings of the 17th DGLR/STAB Symposium, 9.-10. November 2010, Berlin, Germany.

[21] KLIMMEK T., *Parameterization of topology and geometry for the multidisciplinary optimization of wing structures*, Proceedings, European Air and Space Conference, Manchester, 2009.